International Journal of Biological Macromolecules 281 (2024) 136296

Contents lists available at ScienceDirect

International Journal of Biological Macromolecules

journal homepage: www.elsevier.com/locate/ijbiomac

Dependence of the crystal structure on the D-units amount in semi-crystalline poly(lactic acid)

Giovanna Molinari [a,1], Paola Parlanti [b], Elisa Passaglia [c], Federica Aiello [d,e], Mauro Gemmi [b], Andrea Lazzeri [a], Maria Cristina Righetti [d,*]

[a] Department of Civil and Industrial Engineering, University of Pisa, 56122 Pisa, Italy
[b] Center for Materials Interfaces, Istituto Italiano di Tecnologia, 56025 Pontedera, Italy
[c] CNR-ICCOM, National Research Council—Institute of Chemistry of OrganoMetallic Compounds, 56124 Pisa, Italy
[d] CNR-IPCF, National Research Council—Institute for Chemical and Physical Processes, 56124 Pisa, Italy
[e] Center for Instrument Sharing, University of Pisa (CISUP), Lungarno Pacinotti 43, 56126 Pisa, Italy

ARTICLE INFO

Keywords:
Poly(lactic acid)
Copolymer
Crystal structure
Comonomer inclusion

ABSTRACT

The study investigates the impact of the D-lactic acid units content on the crystallinity and crystal structure of commercial poly(lactic acid) (PLA) grades, which are copolymers of poly(L-lactic acid) (PLLA) containing a minor amount of D-units. As the D-units content increases, a detectable decrease in crystallinity was observed along with a simultaneous rise in mobile amorphous fraction (MAF) and a reduction in rigid amorphous fraction (RAF). The percentage of D-units was found not to significantly affect RAF thickness, suggesting that the D-units are not completely excluded from the crystals. The inclusion of D-units as defects in the PLA crystal lattice was confirmed by XRD analysis, which disclosed that the crystal phase gets gradually richer of D-units as the crystallization time evolves. FT-IR analysis proved that the incorporation of D-units in the crystal phase is promoted by the formation of local $CH_3\cdots O{=}C$ interactions, similar to those massively active between PLLA and poly(D-lactic acid) (PDLA) in the stereocomplex. The establishment of these interactions leads to a contraction of the interplanar distances and a decrease in the crystal cell volume with increasing the crystallization time and the D-units percentage. In summary, the study proves that for PLA copolymers containing a D-units percentage at least up to about 8 %, D-units are included in the crystal lattice.

1. Introduction

Poly(lactic acid) (PLA), one of the most investigated bio-based and biodegradable polyester, is a polymer nowadays widely available on the market and extensively employed, especially in the packaging sector [1,2]. PLA can be produced by polycondensation of lactic acid or by ring opening polymerization of lactides, the cyclic dimers of lactic acid [3]. Due to the chiral carbon, lactic acid presents two optically active forms, L-lactic acid and D-lactic acid, whereas the possible dimers are three: LL-lactide, DD-lactide and LD-lactide (or *meso*-lactide). The homopolymers poly(L-lactic acid) (PLLA) and poly(D-lactic acid) (PDLA) comprise exclusively L-lactic acid and D-lactic acid repeating units, respectively, while the term PLA designates copolymers containing both L- and D-units. As the stereoisomer L-lactic acid is the fraction most primarily produced by fermentation of renewable sources [4,5], commercial PLA grades, which mainly derive from L-lactide and DL-lactide, are copolymers of PLLA containing a minor amount of D-units [2,3].

The presence of D-units in the PLA chains strongly affects crystallinity, crystallization rate and melting temperature, which decrease as the D-units content increases [6,7], with the result that PLA copolymers containing >10–15 % of randomly distributed D-units cannot be crystallized and are totally amorphous.

PLLA exhibits a polymorphic behaviour after melt and cold crystallization under normal conditions [8,9]. The most stable PLLA crystal form (α), characterized by two antiparallel left-handed 10_3 helical segments packed in an orthorhombic unit cell, grows at temperatures higher than 120 °C. Crystallization at temperatures lower than 100 °C leads instead to the development of crystals with looser packing and slightly more disordered structure, named α′-crystals, whereas a mixture of α′- and α-crystals grows in the temperature range between 100 and

* Corresponding author.
E-mail address: mariacristina.righetti@cnr.it (M.C. Righetti).
[1] Present address: CNR-IPCF, National Research Council—Institute for Chemical and Physical Processes, 56124 Pisa, Italy.

https://doi.org/10.1016/j.ijbiomac.2024.136296
Received 31 July 2024; Received in revised form 28 September 2024; Accepted 2 October 2024
Available online 4 October 2024
0141-8130/© 2024 The Authors. Published by Elsevier B.V. This is an open access article under the CC BY license (http://creativecommons.org/licenses/by/4.0/).

Table 1
D-units contents declared by the producers and derived from ^{1}H NMR analysis (see Supplementary material) for PLLA and the different PLA grades.

Sample	D-units content declared by the producers	D-units content from ^{1}H NMR analysis
PLLA	0	0
PLA L175	≤1	<1
PLA 4032D	1.6	2.0
PLA 2003D	4.5	4.5
PLA LX930	8	7.8

120 °C [8,9]. The disordered α'-form irreversibly reorganizes/recrystallizes into the more stable α-form if heated at rates lower than 30 K/s above the crystallization temperature [10]. Some extensive discussions can be found in the literature on the mechanism of this transition, whether it is due to melting/recrystallization or a solid-solid transition [11,12]. The temperature of the transition from the α′-region to the α-region shifts to lower temperatures by increasing the D-units content [13–16]. For example, when the D-units content is about 2 %, only α-crystals grow above 105 °C.

The decrease in crystallinity, crystallization rate, melting temperature and lamellar thickness [17,18] with the D-units content increase can be rationalized by assuming that the D-units act as obstacles and defects for the crystallization process. Partial or total rejection of the D-units from the crystal phase has been widely debated in the literature, with controversial and conflicting conclusions [17–21]. Fischer et al. [21] investigated solution grown crystals of PLA copolymers containing D-units up to 10 % and experimentally proved that the D-units are partially included in the PLLA crystal lattice in a percentage that increases with the crystallization temperature and the D-units content. The study also estimated that for a total D-units amount of 10 %, approximately 30 % is included in the crystal phase. Conversely, different studies supported the exclusion of the D-units from the PLLA crystal cell, on the basis of models commonly applied to the analysis of the melting behaviour of random copolymers [18–20], although these models rely on extrapolated quantities (as the equilibrium melting temperature T_m° and the 100 % crystalline enthalpy of melting Δh_m°) and thermodynamic parameters not easily verifiable [19,20,22,23]. It was also proposed that small amount of D-units can initially get stuck within the crystal regions and that prolonged annealing at high temperature may provoke their rejection, with formation of two crystal populations with different stability [17].

With the aim of improving the knowledge and interpretation of the PLA properties, the present study is mainly focused on the crystal structure of some PLA copolymers with different D-units content. In addition, an analysis of the interphase located at the amorphous/crystal boundary is also presented as a function of the D-units content. This nanometric amorphous interphase, called rigid amorphous fraction (RAF), is characterized by segmental mobility slower than that of the amorphous region far from the crystals, which is named mobile amorphous fraction (MAF) [24]. RAF can develop during crystallization, especially at low temperatures, or upon cooling after crystallization, due to the progressively increasing constraints experienced by the amorphous segments close to the crystals as a consequence of the reduced chain mobility [25,26]. Thus, vitrification/devitrification of the rigid amorphous fraction occurs at temperatures higher than the glass transition temperature (T_g) of the MAF. It is also well-known that some properties of the RAF (i.e.: mechanical and permeability features) are different from those of the MAF [27]. Several experimental and theoretical studies have proven that the elastic modulus of the RAF is higher than that of the MAF, thus attesting that the constrained interphase contributes with its peculiarities to the overall mechanical properties of the semi-crystalline material [28–30]. It is therefore crucial to investigate and quantify the RAF present in PLA copolymers as a function of the D-units amount, to gain a more detailed comprehension of its influence on the macroscopic PLA behaviour.

2. Materials and methods

2.1. Materials and preparation

The homopolymer PLLA (0 % D-unit) was purchased from Polysciences Inc. (USA). As copolymers, the following PLA grades were utilized: (*i*) PLA Luminy L175, with D-units content ≤1 % [31], kindly provided by Totalenergies Corbion (The Netherlands), (*ii*) PLA Ingeo 4032D, with 1.6 % of D-units [32], purchased from NatureWorks (USA), (*iii*) PLA Ingeo 2003D, with 4.5 % of D-units [32], purchased from NatureWorks (USA) and (*iv*) PLA Luminy LX930, with 8 % of D-units [33], purchased from Totalenergies Corbion (The Netherlands). To confirm the D-units contents declared by the producers, ^{1}H NMR experiments were conducted for the different PLA grades. This analysis is described in the Supplementary material. The ^{1}H NMR results were found in very good agreement with the D-units percentages declared by the producers, as attested by the data listed in Table 1.

Initially, the as-received PLLA powder and PLA granules were dried in a DP604–615 PIOVAN dryer (Venezia, Italy) at 60 °C for 24 h. Films of PLLA and the different PLA grades with average thickness of approximately 150–200 μm were prepared by means of a press Carver bench model 3851 CE (Wabash, IN, USA). The dried powder and granules were placed between the two hot plates of the press and held at 180 °C under a pressure of 10–20 kg/cm^2 for 2 min. Successively, the films were quickly cooled to room temperature, to obtain amorphous samples.

2.2. Size exclusion chromatography (SEC) analysis

Size exclusion chromatography analysis was performed using an Agilent Technologies 1260 Series instrument (Agilent, Santa Clara, CA, USA) equipped with a degasser, an isocratic HPLC pump, a refractive index (RI) detector, a PLgel 5 μm pre-column, and two PLgel MiniMIX-D 5 μm columns (Agilent, Santa Clara, CA, USA) conditioned at 35 °C. $CHCl_3$ for HPLC was used as the eluent at a flow rate of 0.3 mL/min. The system was calibrated with polystyrene standards in a range from 500 to 3×10^5 g/mol. The samples were dissolved in $CHCl_3$ (3 mg/mL) and filtered through a 0.20 μm syringe filter before analysis. The number-average molar mass (M_n) and the mass-average molar mass (M_w) were calculated using Agilent ChemStation software (OpenLab Control Panel version A0104, Agilent Technologies, Santa Clara, CA, USA).

2.3. Thermal characterization by Differential Scanning Calorimetry (DSC) and Temperature-Modulated Differential Scanning Calorimetry (TMDSC)

DSC and TMDSC measurements were performed with a PerkinElmer Calorimeter DSC 8500 equipped with an IntraCooler III as refrigerating system (PerkinElmer, Waltham, MA, USA). The instrument was calibrated in temperature with high-purity standard materials (indium, naphthalene, and cyclohexane) according to the procedure for conventional DSC [34]. Enthalpy calibration was performed with indium. Each scan was accompanied by an empty pan run (blank run). The mass of the blank and sample aluminium pans matched within 0.02 mg. To minimize the instrumental thermal lag, the sample mass was about 10 mg. Dry nitrogen was used as purge gas at a rate of 20 mL/min. The

temperature of the samples upon heating was corrected for the thermal lag, determined as average value by using different standard materials. This lag was 0.05 min, which, for the heating rates of 2 and 10 K/min, corresponds to a temperature correction of −0.1 and −0.5 K, respectively.

As preliminary investigation, the thermodynamic specific heat capacities of PLLA and the different PLA grades in the solid and liquid state ($c_{p,s}$ and $c_{p,l}$, respectively) were measured by TMDSC from 20 to 195 °C by utilizing the amorphous films. To this purpose, to erase the thermal history of the samples, each TMDSC run was preceded by a heating run at 20 K/min up to 190 °C, followed by an isotherm of 4 min and then a quick cooling to 20 °C (effective cooling rate: 130 K/min). The TMDSC measurements were performed by utilizing a saw-tooth modulation temperature program, at the average heating rate of 2 K/min, with a temperature amplitude (A_T) of 0.5 K and a modulation period (p) of 120 s. According to the mathematical treatment of TMDSC data, the modulated temperature and heat flow rate curves can be approximated to discrete Fourier series and separated into average and periodic components [35,36]. The average components are equivalent to the conventional linear temperature program and the corresponding conventional heat flow rate signal, from which the $c_{p,ave}$ curve can be derived. Conversely, from the periodic component, the $c_{p,rev}$ curve can be calculated according to Eq. (1):

$$c_{p,rev}(\omega, T) = \frac{A_{HF}(T)}{A_T(T)} \frac{K(\omega)}{m\omega} \quad (1)$$

where A_{HF} and A_T are the amplitudes of the first harmonic of the modulated heat flow and temperature, respectively, ω is the fundamental frequency of temperature modulation ($\omega = 2\pi/p$), m is the mass of the sample, and $K(\omega)$ is the frequency-dependent calibration factor. The average $K(\omega)$ value, determined by calibration with sapphire, was 1.00 ± 0.02 for $p = 120$ s.

The enthalpy of melting of 100 % crystalline PLLA (Δh_m°) was determined by measuring the enthalpy of isothermal crystallization (Δh_c) at the crystallization temperatures (T_c) of 124, 126 and 128 °C (crystallization times: 40, 45 and 50 min, respectively), and the corresponding enthalpy of melting (Δh_m), by heating the samples directly from T_c to 195 °C at 10 K/min. Before crystallization, to erase the previous thermal history, the samples were heated at 20 K/min up to 190 °C, maintained at 190 °C for 4 min, and then quickly cooled to the various T_cs.

Semi-crystalline PLLA and PLA samples were prepared in DSC. The samples, taken from the amorphous films, were heated at 190 °C, maintained at this temperature for 4 min, and then quickly cooled to the following T_cs: 130 °C for PLLA, 120 °C for PLA L175, PLA 4032D and PLA 2003D, and 90 °C for PLA LX930. The crystallization times were 25 min and 2 h for PLLA; 1 h and 2 h for PLA L175; 25 min, 2 h and 48 h for PLA 4032D; 3 h, 48 h and 96 h for PLA 2003D; 16 h, 48 h and 96 h for PLA LX930. The thermal treatments were chosen to produce PLA samples containing exclusively α-crystals with different crystallinity degrees, by taking into account also the respective crystallization rates.

After crystallization, the PLLA and PLA samples were quickly cooled to 20 °C and analysed from 20 to 195 °C (*i*) by DSC at 10 K/min, to obtain apparent specific heat capacity ($c_{p,app}$) curves, and (*ii*) by TMDSC at 2 K/min, with $A_T = 0.5$ °C and $p = 120$ s, to attain the $c_{p,rev}$ curves. From the $c_{p,rev}$ curves, the mobile amorphous fractions at the end of the glass transition temperatures were estimated, whereas the crystal weight fractions were determined from the Δh_m values, determined by integration of the $c_{p,app}$ curves in the melting region, by assuming a linear baseline from the relative T_c to the end of the melting process.

2.4. X-ray diffraction (XRD) analysis

XRD data were acquired in transmission/Debye-Scherrer geometry using a STOE Stadi P diffractometer (Darmstadt, Germany) equipped with Cu tube monochromated on the Cu-Kα1 radiation (λ = 1.5406 Å) by a Ge (1 1 1), a Johansson monochromator and a MYTHEN2 1 K detector from Dectris. The line focused Cu X-ray tube was operated at 40 kV and 40 mA. For the XRD analysis, three disks cut from the amorphous PLLA and PLA films were stacked in DSC aluminium pans, to obtain samples with diameter of about 5 mm and thickness of about 0.5 mm. The amorphous and semi-crystalline PLLA and PLA samples were prepared in DSC according to the thermal histories described in the previous section. Data were acquired in the 2θ range 2–60° (maximum resolution ca. 1.5 Å) with a step of 0.03° between consecutive points. A scan without samples was performed and subtracted from each scan, to avoid the air and incoherent scattering contributions. The X-ray crystalline fractions (X_C^{XRD}) were calculated as the ratio between the areas of the crystalline peaks and the total area of the background corrected diffraction profile. The lattice constants were calculated from the positions of the most intense XRD peaks of the PLA α-form by means of the software WinxPow (STOE, Darmstadt, Germany).

Table 2
Number-average molar mass (M_n) and mass-average molar mass (M_w) of the as-received PLLA and PLA samples.

Sample	$M_n/10^4$ [g/mol]	$M_w/10^4$ [g/mol]
PLLA	7.9	12.0
PLA L175	11.0	17.8
PLA 4032D	12.2	19.9
PLA 2003D	13.0	20.6
PLA LX930	10.3	17.5

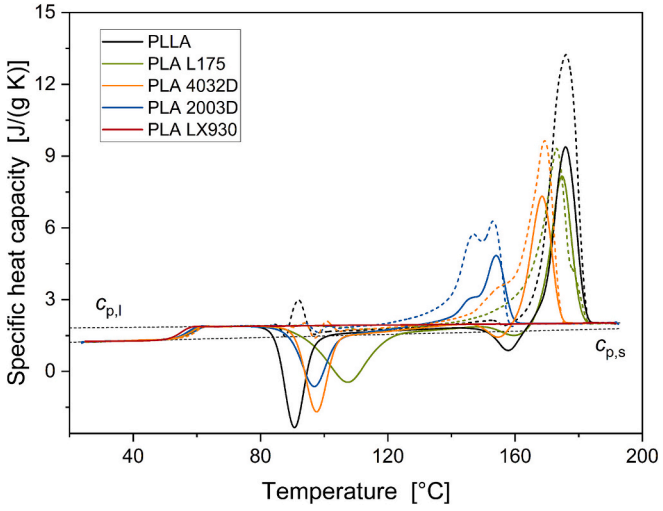

Fig. 1. Reversing and average specific heat capacity curves ($c_{p,rev}$ and $c_{p,ave}$, dashed lines and solid lines, respectively) of amorphous PLLA and PLA copolymers at 2 K/min. The black dotted lines are the thermodynamic solid and liquid specific heat capacities ($c_{p,s}$ and $c_{p,l}$).

2.5. FT-IR analysis

Infrared spectra (FT-IR) were recorded with a Fourier Transform Spectrometer Perkin Elmer Spectrum Two (PerkinElmer, Waltham, MA, USA) in the 400–4000 cm^{-1} range with a resolution of 4 cm^{-1} using 132 scans. Spectra of PLLA and PLA LX930 amorphous samples were carried on films obtained by solution casting on KBr discs. About 60 mg of polymer were dissolved in 4 mL of $CHCl_3$ and 5 drops of the resulting solution deposited on the KBr. The analysis was then performed after the solvent evaporation. The spectra of the semi-crystalline PLLA and PLA LX930 samples were recorded in the same manner after treatment of the films deposited on KBr discs at 130 °C for 2 h in the case of PLLA and at 90 °C for 48 h in the case of PLA LX930.

Table 3
Glass transition temperature of amorphous ($T_{g,am}$) PLLA and PLA copolymers determined from the $c_{p,rev}$ curves. Glass transition temperature ($T_{g,sc}$) determined from the $c_{p,rev}$ curves; mobile amorphous weight fraction (w_{MAF}); melting temperature assumed as the temperature of the highest melting peak (T_m) measured at 10 K/min; enthalpy of melting (Δh_m) at T_m measured at 10 K/min; crystalline weight fraction (w_C); rigid amorphous weight fraction (w_{RAF}); w_{RAF}/w_C ratio; crystalline weight fraction calculated by XRD (X_C^{XRD}) for semi-crystalline PLLA and PLA copolymers (±0.5 °C for T_g; ±0.2 °C for T_m; ±0.4 J/g for Δh_m; ±0.02 for w_{MAF}; ±0.03 for w_C; ±0.05 for w_{RAF}; ±0.02 for X_C^{XRD}).

Sample	Thermal treatment	$T_{g,am}$ [°C]	$T_{g,sc}$ [°C]	w_{MAF}	T_m [°C]	$\Delta h_m(T_m)$ [J/g]	w_C	w_{RAF}	w_{RAF}/w_C	X_C^{XRD}
PLLA	Amorphous	60.0		1	–	–	0	0	–	0
	T_c = 130 °C 25 min		64.0	0.28	174.7	60.0	0.42	0.30	0.67	0.42
	T_c = 130 °C 2 h		64.5	0.27	176.0	62.5	0.44	0.29	0.67	0.44
PLA L175	Amorphous	59.5		1	–	–	0	0	–	0
	T_c = 120 °C 1 h		61.5	0.36	171.1	52.3	0.37	0.27	0.71	0.36
	T_c = 120 °C 2 h		63.0	0.36	172.7	53.6	0.38	0.26	0.71	0.37
PLA 4032D	Amorphous	59.0		1	–	–	0	0	–	0
	T_c = 120 °C 25 min		60.0	0.43	166.2	44.6	0.32	0.25	0.71	0.31
	T_c = 120 °C 2 h		61.5	0.41	167.8	48.7	0.35	0.24	0.68	0.34
	T_c = 120 °C 48 h		63.0	0.39	168.1	52.8	0.37	0.24	0.66	0.36
PLA 2003D	Amorphous	58.5		1	–	–	0	0	–	0
	T_c = 120 °C 3 h		58.0	0.50	154.2	39.2	0.29	0.21	0.71	0.29
	T_c = 120 °C 48 h		58.5	0.47	156.8	43.2	0.32	0.21	0.66	0.32
	T_c = 120 °C 96 h		59.5	0.46	157.3	44.5	0.33	0.21	0.67	0.33
PLA LX930	Amorphous	55.0		1	–	–	0	0	–	0
	T_c = 90 °C 16 h		55.0	0.94	129.0	4.9	0.04	0.02	0.50	0.05
	T_c = 90 °C 48 h		55.5	0.75	130.0	19.7	0.16	0.09	0.76	0.17
	T_c = 90 °C 96 h		56.0	0.58	131.6	29.5	0.24	0.18	0.74	0.23

3. Results and discussion

3.1. Size exclusion chromatography (SEC) analysis

The number-average molar mass (M_n) and the mass-average molar mass (M_w) values of the as-received PLLA, PLA L175, PLA 4032D, PLA 2003D and PLA LX930, measured by size exclusion chromatography, are listed in Table 2. The M_n and M_w values are substantially similar for all the samples, which means that a direct comparison between the properties of the different grades is practicable.

3.2. Thermodynamic characterization: solid and liquid specific heat capacities of PLLA and PLA copolymers and enthalpy of melting of 100 % crystalline PLLA

The thermodynamic solid and liquid specific heat capacities ($c_{p,s}$ and $c_{p,l}$) of PLLA and the PLA grades with various D-units amount were estimated from several repeated $c_{p,rev}$ curves in the glassy and liquid regions. Fig. 1 shows the reversing and average specific heat capacity ($c_{p,rev}$ and $c_{p,ave}$) curves of the initially amorphous PLLA and PLA copolymers at the average heating rate of 2 K/min. The dotted lines, constructed by extrapolating the $c_{p,rev}$ data from below the glass transition and by linearly linking the melt to the region above T_g, are common to all the samples. This proves that the derived $c_{p,s}$ and $c_{p,l}$ expressions, $c_{p,s} = 1.16 + 0.0033 \cdot T$ and $c_{p,l} = 1.80 + 0.0012 \cdot T$, with $c_{p,s}$ and $c_{p,l}$ in J/(g K) and T in °C, apply for all the samples (estimated error: ± 0.02 J/(g K). These values differ <5 % from the $c_{p,s}$ and $c_{p,l}$ data previously reported in literature [37].

The glass transition of the amorphous PLLA and PLA copolymers ($T_{g,am}$) lies in the range 60–55 °C, as shown in Table 3. $T_{g,am}$ slightly decreases with the increase of D-units content, in agreement with literature data [6]. Above the glass transition, the $c_{p,ave}$ curves display a cold crystallization process. In correspondence of the cold crystallization event, the $c_{p,rev}$ curves display irregular oscillations, which can be considered as artefacts connected to the fast release of crystallization latent heat [38]. Cold crystallization of the PLA copolymers occurs at higher temperatures with respect to the homopolymer, due to the lower crystallization tendency of the copolymers with respect to PLLA [6]. During cold crystallization of PLLA, PLA L175 and PLA 4032D, α′-crystals are produced [9], as attested by the exothermic peak present

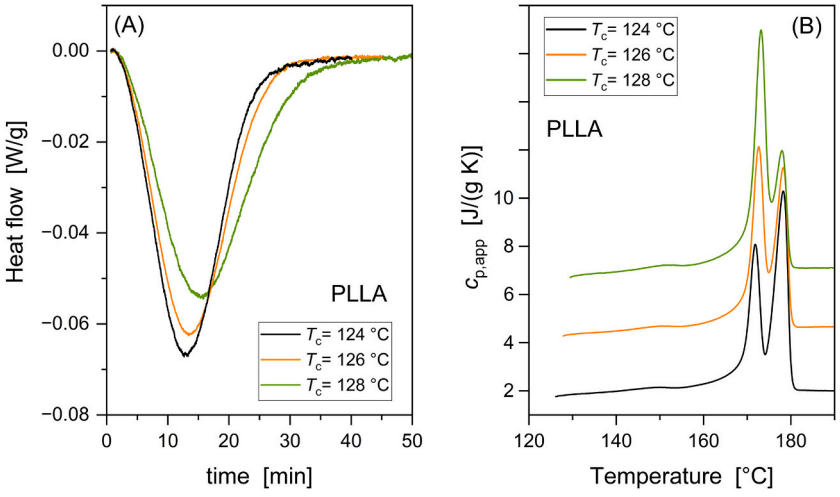

Fig. 2. (A) Heat flow rate during isothermal crystallization of PLLA at the indicated T_cs; (B) Apparent specific heat capacity ($c_{p,app}$) of PLLA as a function of temperature at 10 K/min after isothermal crystallization at the indicated T_cs. The ordinate values refer only to the bottom curve. The other curves are shifted vertically for the sake of clarity.

Table 4
Crystallization temperature (T_c); enthalpy of crystallization (Δh_c) at T_c; melting temperature assumed as the average temperature of the melting endotherm measured at 10 K/min (T_m); enthalpy of melting (Δh_m) at T_m measured at 10 K/min; crystalline weight fraction (w_C) calculated from Eq. (4); enthalpy of melting of 100 % crystalline PLLA at T_m (Δh_m° (T_m)) (estimated error: ±0.2 °C for T_m; ±0.6 J/g for Δh_c; ±0.4 J/g for Δh_m; ±0.05 for w_C; ±15 J/g for Δh_m°).

Sample	T_c [°C]	Δh_c (T_c) [J/g]	T_m [°C]	Δh_m (T_m) [J/g]	w_C	Δh_m° (T_m) [J/g]
PLLA	124	−51.7	175	58.6	0.41	141
PLLA	126	−52.5	175	59.1	0.42	142
PLLA	128	−54.4	175	60.9	0.43	142

in the $c_{p,ave}$ curves in the range 150–160 °C, which is connected to the α'-crystals reorganization into the α-form [10,12,39,40]. The absence of the exothermic peak in the $c_{p,ave}$ curve of PLA 2003D proves that only α-crystals grow during cold crystallization, because the transition from the α′-region to the α-region shifts to lower temperatures by increasing the D-units content [13–16]. The copolymer with the higher D-units content, PLA LX930, does not undergo cold crystallization even at 2 K/min. The melting temperature of the crystals progressively moves to lower temperatures by increasing the D-units amount, as already reported [6].

The accurate thermodynamic solid and liquid specific heat capacities were utilized for the quantification of the enthalpy of melting of 100 % crystalline PLLA (Δh_m°) by means a thermodynamic method never utilized before for PLLA. Literature values of Δh_m° for PLLA vary in a wide range (90–200 J/g) [41]. By coupling data from DSC and X-ray diffraction experiments, a Δh_m° value of 143 J/g at the melting temperatures of 180 °C was proposed for the α-crystals [41]. However, the enthalpy of melting of 100 % crystalline PLLA with α-crystals is a topic still under debate, as proved by a quite recent publication [42]. Thus, additional verification of the more correct Δh_m° value for the α-form was here performed by combining crystallization and melting enthalpy data. The derivation of the thermodynamic equation utilized for this purpose is here described.

The crystalline weight fraction (w_C) of a sample crystallized at a given crystallization temperature (T_c) can be calculated from the absolute value of the enthalpy of isothermal crystallization (Δh_c) at T_c or the enthalpy of melting (Δh_m) at the melting temperature (T_m), being $\Delta h_m(T) = -\Delta h_c(T)$, through the following equation:

$$w_C = \frac{|\Delta h_c(T_c)|}{\Delta h_m^\circ(T_c)} = \frac{\Delta h_m(T_m)}{\Delta h_m^\circ(T_m)} \quad (2)$$

From the relationship that links $\Delta h_m^\circ(T_m)$ to $\Delta h_m^\circ(T_c)$:

$$\Delta h_m^\circ(T_m) = \Delta h_m^\circ(T_c) + \int_{T_c}^{T_m} \Delta c_p(T)\mathrm{d}T \quad (3)$$

with $\Delta c_p = c_{p,l} - c_{p,s} = a - bT$, the following equation can be derived:

$$w_C = \frac{\Delta h_m(T_m) - |\Delta h_c|(T_c)}{a(T_m - T_c) - \frac{b}{2}\left(T_m^2 - T_c^2\right)} \quad (4)$$

From Eq. (4) w_C can be determined without the utilization of Δh_m° values. As a second step, from the w_C value, $\Delta h_m^\circ(T_c)$ and $\Delta h_m^\circ(T_m)$ can be deduced through Eq. (2) from the experimental Δh_c and Δh_m data.

Fig. 2 shows the heat flow rate signals during isothermal crystallization at different T_cs and the successive melting behaviour of PLLA. The absence of the exothermic peak in the range 150–160 °C attests that only α-crystals grow at the T_cs investigated. The experimental Δh_c and Δh_m data and the w_C and Δh_m° values at the relative T_ms, calculated by means of Eqs. (2)–(4) by assuming $a = 0.64$ J/(g K) and $b = 0.0021$ J/(g K^2), are collected in Table 4. By considering the estimated error, the enthalpy of melting of 100 % crystalline PLLA with α-crystals is around 140 J/g, in perfect agreement with the previous study [41].

3.3. Thermal characterization: determination of the phase composition of the semi-crystalline PLLA and PLA copolymers

Fig. 3 shows the reversing specific heat capacity ($c_{p,rev}$) curves of the semi-crystalline PLLA and PLA copolymers at the average heating rate of 2 K/min, together with the apparent specific heat capacity ($c_{p,app}$) curves at the heating rate of 10 K/min after crystallization according to the following thermal treatments: $T_c = 130$ °C (25 min and 2 h) for PLLA; $T_c = 120$ °C (1 h and 2 h) for PLA L175; $T_c = 120$ °C (25 min, 2 h and 48 h) for PLA 4032D; $T_c = 120$ °C (3 h, 48 h and 96 h) for PLA 2003D and $T_c = 90$ °C (16 h, 48 h and 96 h) for PLA LX930. The glass transition temperatures of semi-crystalline PLLA and PLA samples ($T_{g,sc}$), derived from the $c_{p,rev}$ curves, progressively shift to higher temperatures with increasing the crystallization time. After prolonged crystallization times, $T_{g,sc}$ values are higher than the corresponding $T_{g,am}$ values (as shown in Table 3). In any case, $T_{g,sc}$ decreases as the D-content raises like for the amorphous samples. As already reported, also the melting temperature T_m shifts to lower temperatures with increasing the D-content [6]. The total absence of the exothermal process before melting proves that only α-crystals are present in the isothermally crystallized PLLA and PLA copolymers.

The mobile amorphous fractions (w_{MAF}) were calculated for all the samples at the end of the glass transition as $w_{MAF} = (c_{p,rev} - c_{p,s})/(c_{p,l} - c_{p,s})$. The crystalline weight fractions (w_C) were calculated as $w_C = \Delta h_m(T_m)/\Delta h_m^\circ(T_m)$, with $\Delta h_m^\circ(T_m)$ calculated according to the $\Delta h_m^\circ(T)$ expression previously quantified [41]. Finally, the rigid amorphous fractions (w_{RAF}) were derived by difference: $w_{RAF} = 1 - w_C - w_{MAF}$. All the w_{MAF}, w_C and w_{RAF} values are listed in Table 3. These data show that the decrease in crystallinity, expected with the D-units increase [6], is correlated with a rise in MAF and a decrease in RAF. For comparison, the crystalline weight fractions of all the samples determined by XRD analysis (X_C^{XRD}) (see section below) are also reported in Table 3. The very good agreement between the crystallinity values determined by means of two different techniques confirms the accuracy of the Δh_m° values utilized for the calculation of w_C.

The w_{RAF}/w_C ratio, which is listed in Table 3, can be considered as the average RAF amount for crystal unit [43]. It can be observed that w_{RAF}/w_C ratio remains constant or decreases with increasing the crystallization time for PLLA and the PLA copolymers up to PLA 2003D. This trend is in agreement with the general RAF evolution: both RAF and w_{RAF}/w_C generally increase during the crystallization process, reaching a maximum and then slightly decrease in parallel to the final crystallization and progressive perfection of the crystals [43,44]. Conversely, for PLA LX930 the increase in w_{RAF}/w_C ratio detected from 0.50 after 16 h to 0.76 after 48 h at 90 °C can be rationalized by considering that crystallization is still in progress, as proven by the low w_C values. However, the w_{RAF}/w_C ratio values are quite similar for PLLA and PLA copolymers, which seems to indicate that the D-units do not substantially impact on RAF thickness. This result can lead to considerations on the RAF composition. For copolymers in which the comonomer is rejected from the crystal phase, it has been reported that the excluded comonomers accumulate at the crystal basal planes, with formation of a RAF layer that changes its composition and thickness as a function of comonomer percentage [45]. The present data on the RAF of PLA copolymers, which appear independent of the D-units amount, seem to suggest that the D-units are not completely excluded from the crystals. To verify this

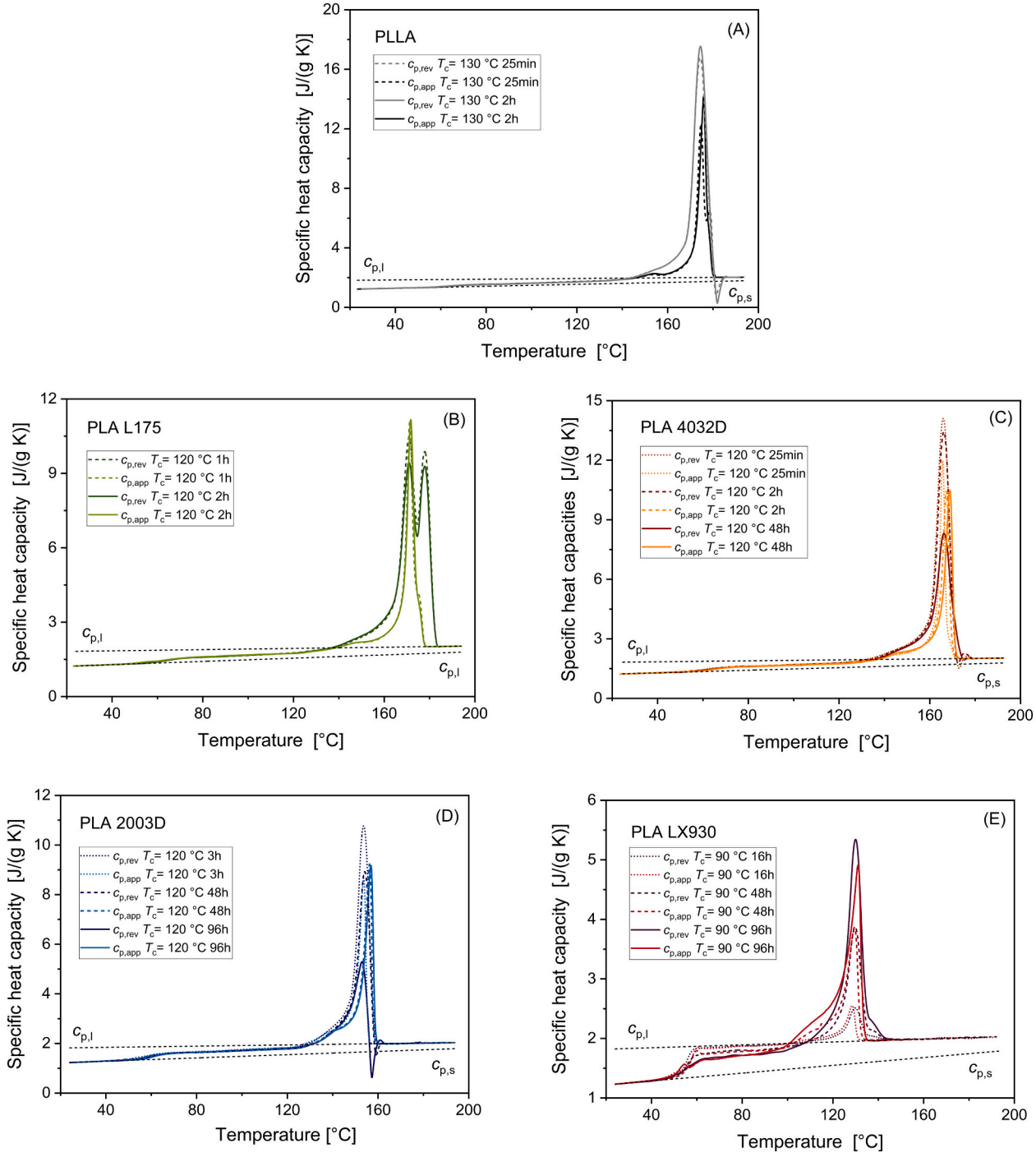

Fig. 3. Reversing specific heat capacity curves ($c_{p,rev}$) at 2 K/min and apparent specific heat capacity curves ($c_{p,app}$) at 10 K/min of PLLA and the PLA copolymers crystallized according to the following thermal treatments: (A) PLLA: T_c = 130 °C (25 min and 2 h); (B) PLA L175: T_c = 120 °C (1 h and 2 h); (C) PLA 4032D: T_c = 120 °C (25 min, 2 h and 48 h); (D) PLA 2003D: T_c = 120 °C (3 h, 48 h and 96 h); (E) PLA LX930: T_c = 90 °C (16 h, 48 h and 96 h). The black dotted lines are the thermodynamic solid and liquid specific heat capacities ($c_{p,s}$ and $c_{p,l}$), respectively.

hypothesis, a detailed investigation by means of XRD analysis was conducted on PLLA and PLA copolymers.

3.4. XRD analysis

The XRD patterns of the semi-crystalline PLLA and PLA copolymers with the respective highest crystallinities, obtained at room temperature, are shown in Fig. 4. PLLA exhibits the profile uniquely belonging to the α-phase, easily identified by the position of the most intense (110/200) and (203/113) peaks at the 2θ scattering angles of 16.6° and 19.0° and the (103/004), (011) and (211) peaks at 12.5°, 14.7° and 22.3°, as well as for several other less intense reflections at higher angles [41].

Remarkably, the XRD peaks shift towards slightly higher 2θ values with increasing the D-units amount: the change for the most intense peak is about +0.12° for PLA 4032D and + 0.18° for PLA 2003D. This behaviour indicates structural contraction towards lower interplanar distances and lattice dimensions. The profile of the PLA LX930 is indeed peculiar: the (110/200) peak appears double, with one peak centred at a 2θ value slightly higher than that typical of pure PLLA and another peak at even higher 2θ. Both peaks however move to higher 2θ values with

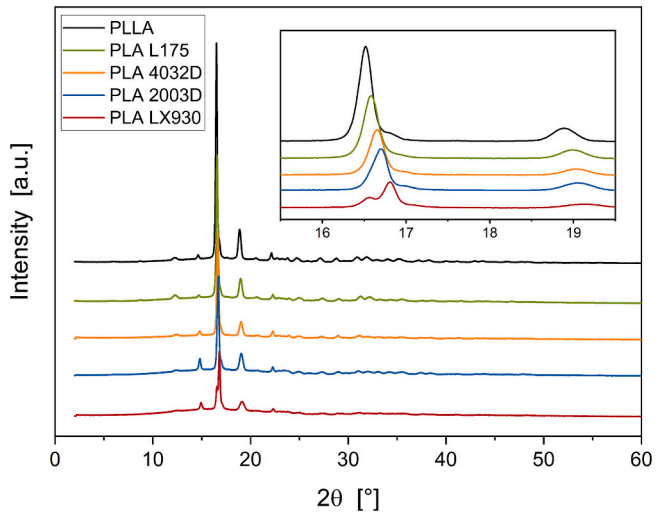

Fig. 4. XRD patterns of PLLA and the various PLA copolymers crystallized according to the following thermal treatments: $T_c = 130$ °C (2 h) for PLLA; $T_c = 120$ °C (2 h) for PLA L175; $T_c = 120$ °C (48 h) for PLA 4032D; $T_c = 120$ °C (96 h) for PLA 2003D and $T_c = 90$ °C (96 h) for PLA LX930. The inset is an enlargement.

increasing the crystallization time.

Fig. 5(A), (B), (C) and (D) displays the (110/200) reflections, normalized to the relative highest value, for PLLA, PLA L175, PLA 4032D and PLA 2003D after crystallization for different times. (The change in crystallinity for each of these samples after the different crystallization times is small.) For comparison, the (110/200) reflection of PLLA is also reported. Fig. 5(E) shows the (110/200) peaks for PLA LX930 normalized to the highest value of the PLLA peak. It can be observed that the peak (110/200) of PLA L175, PLA 4032D and PLA 2003D shifts towards higher 2θ values with increasing the D-content and the crystallization time, as well as the two (110/200) reflections of PLA LX930, whose intensity also progressively increases in parallel with a substantial change in crystallinity, as reported in Table 3.

Quantitative analysis of the *d*-spacings linked to the most intense peaks was performed. The results are plotted in Fig. 6(A), (B) and (C) as a function of the D-units content. For PLA LX930, the plotted d_{200} spacings refer to the reflection at higher 2θ values.

The trends of the d_{011}, d_{200} and d_{203} spacings indicate clearly that the interplanar distances shrink with increasing the D-units content. From the position of the most intense peaks, a further investigation was performed to determine the average crystallographic parameters of the α-phase of PLLA and PLA copolymers. (For PLA LX930, the lattice parameters were obtained from the position of the reflection (110/200) at higher 2θ values.) The average crystallographic parameters were derived for the orthorhombic cell of PLA α-phase. The interplanar distances (d_{hkl}) were calculated according to the Bragg's law ($n\lambda = 2d_{hkl}\sin\theta$), and used to obtain the dimensions of the crystalline PLA cell through the equations [46]:

$$(d_{hkl})^{-2} = (h/a)^2 + (k/b)^2 + (l/c)^2 \quad (5)$$

Table 5 lists the orthorhombic cell dimensions and the corresponding estimated cell volumes for PLLA and the PLA copolymers.

Table 5 discloses that for each sample the lattice parameters *a*, *b* and *c* slightly decrease with the crystallization time. A contraction of the unit cell parameters and volume during crystallization is generally ascribed to crystals perfection [47]. More importantly, Table 5 shows that the lattice parameters and the volume cell decrease with increasing the D-

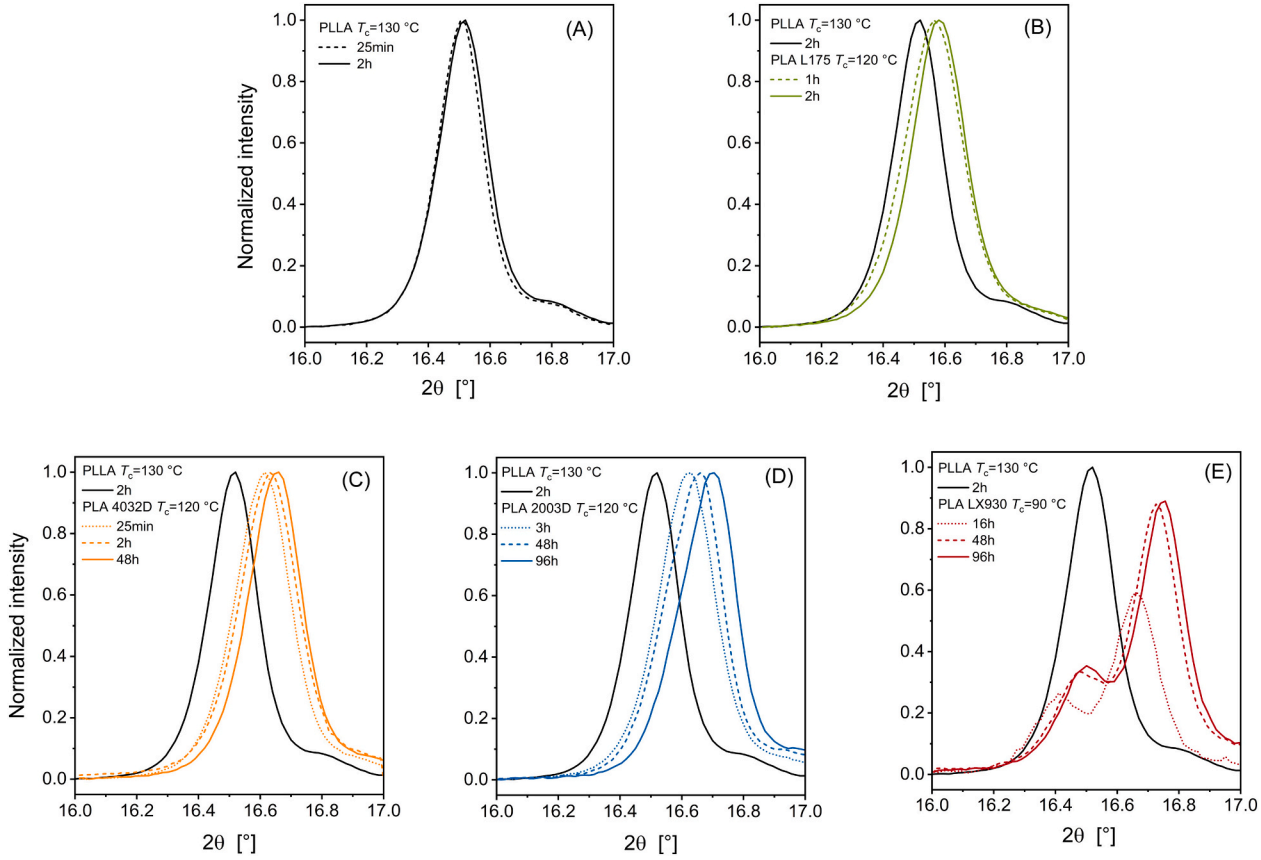

Fig. 5. Normalized XRD profiles of the (110/200) peak for (A) PLLA, (B) PLA L175, (C) PLA 4032D, (D) PLA 2003D and (E) PLA LX930 after crystallization for different times (see legends).

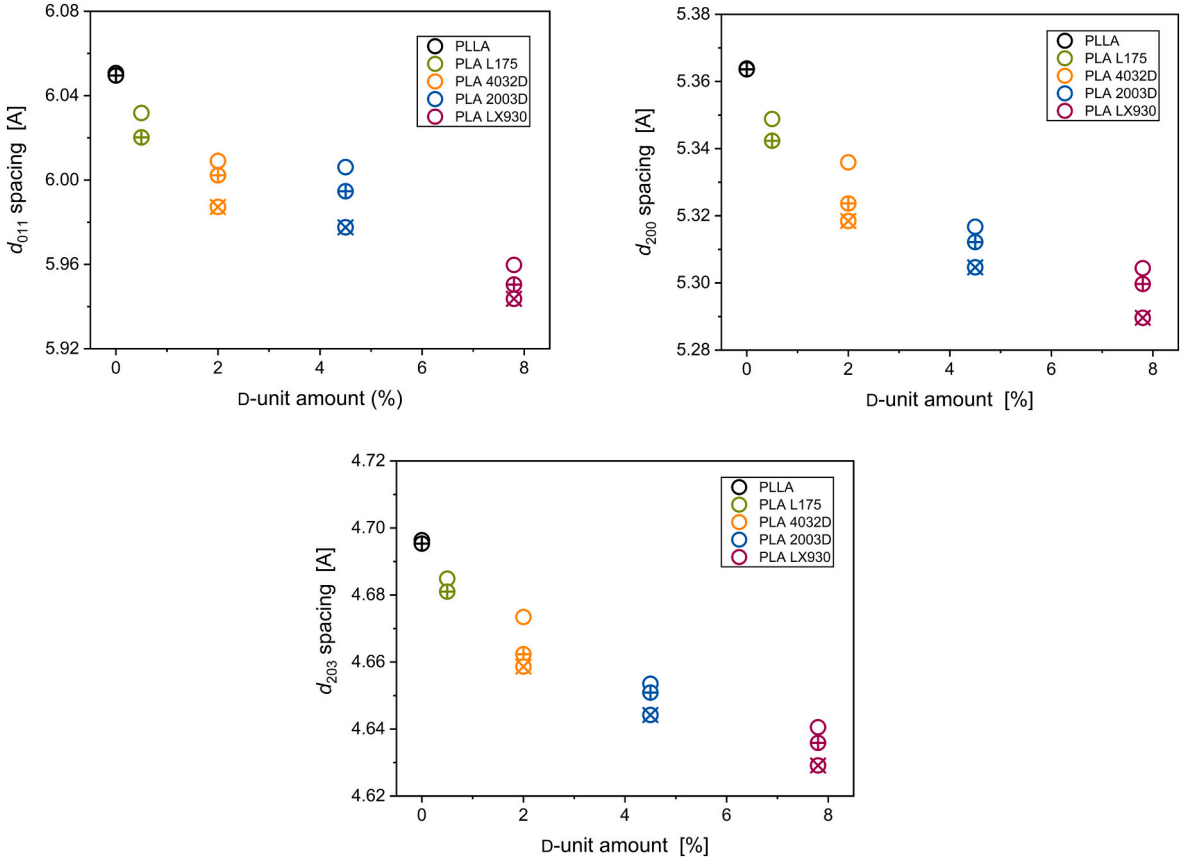

Fig. 6. Dependence of the d_{011}, d_{200} and d_{203} spacings for semi-crystalline PLLA and PLA copolymers after increasing crystallization times (in the order ○ ⊕ ⊗) as a function of the D-units amount (Y-axis units: angstrom).

Table 5
Unit cell parameters and cell volume of PLLA and the PLA copolymers after crystallization according to the thermal treatment indicated.

Sample	Thermal treatment	*a* [Å]	*b* [Å]	*c* [Å]	Cell volume [Å^3]
PLLA	T_c = 130 °C 25 min	10.73	6.07	29.16	1900
	T_c = 130 °C 2 h	10.73	6.07	29.14	1897
PLA L175	T_c = 120 °C 1 h	10.70	6.05	29.13	1886
	T_c = 120 °C 2 h	10.68	6.04	29.13	1881
	T_c = 120 °C 25 min	10.67	6.03	29.05	1870
PLA 4032D	T_c = 120 °C 2 h	10.65	6.02	28.98	1858
	T_c = 120 °C 48 h	10.64	6.01	28.97	1852
	T_c = 120 °C 3 h	10.63	6.03	28.88	1851
PLA 2003D	T_c = 120 °C 48 h	10.62	6.02	28.87	1846
	T_c = 120 °C 96 h	10.61	6.00	28.83	1834
	T_c = 90 °C 16 h	10.61	6.00	28.74	1829
PLA LX930	T_c = 90 °C 48 h	10.60	5.99	28.70	1823
	T_c = 90 °C 96 h	10.54	5.98	28.70	1816

units content.

To the best of our knowledge, analysis of the PLA cell dimensions as a function of the D-units amount has never been previously reported. Thus, for the first time the present study reports structural data of PLA copolymers as a function of D-units content. The structural evolution quantified in Table 5 can be interpreted by assuming partial inclusion of D-units in the crystal phase, with formation of local interactions like those active in the poly(L-lactide)/poly(D-lactide) (PLLA/PDLA) stereocomplex and ascribable to $CH_3\cdots O{=}C$ interactions [48–51]. This type of interaction, which is weak in PLLA [52] and stronger and massively present in the stereocomplex, where L-units and D-units are packed side by side, can be active locally and in small percentage also in the PLA copolymers. These local additional interactions in the crystal phase of the PLA copolymers can thus lead to crystalline structures slightly more compact and with smaller volume.

The gradual shift of the XRD peaks towards higher 2θ values, detectable for PLA L175, PLA 4032D and PLA 2003D reveals also that the D-units inclusion occurs progressively and that the crystal phase gets gradually richer in D-units as the crystallization time evolves. As previously reported, PLLA α-crystals chains perform helical jump motions at temperatures higher than 115 °C [53,54]. This molecular dynamics could trigger the progressive inclusion of D-units in the crystal lattice of PLA L175, PLA 4032D and PLA 2003D, with formation of more compact crystal structures due to the additional interactions between L- and D-units.

The XRD behaviour of the copolymer PLA LX930 is different. The presence of two (110)/(200) reflections could result from a non-totally random copolymer, with crystallization of two different crystal phases, one with a lower percentage and the other one with a higher percentage of D-units, or could be due to the fact that crystallization of this copolymer was carried out at 90 °C. The crystalline helical jump motions could be more hindered at a lower temperature, which means that D-units incorporation in the PLA lattice could occur less easily and more slowly, with also formation of crystalline regions less rich in D-units. The detailed study of the peculiar XRD behaviour and crystal structure of the commercial PLA LX930 is however out of the scope of the present study, which aims to prove that D-units enter the crystal phase of PLA copolymers containing at least up to about 8 % of D-percentage.

3.5. FT-IR analysis

To investigate and confirm the possible presence of specific interactions between the D- and L-units in the crystal phase of the PLA copolymers, FT-IR analysis was performed on semi-crystalline PLLA and PLA LX930.

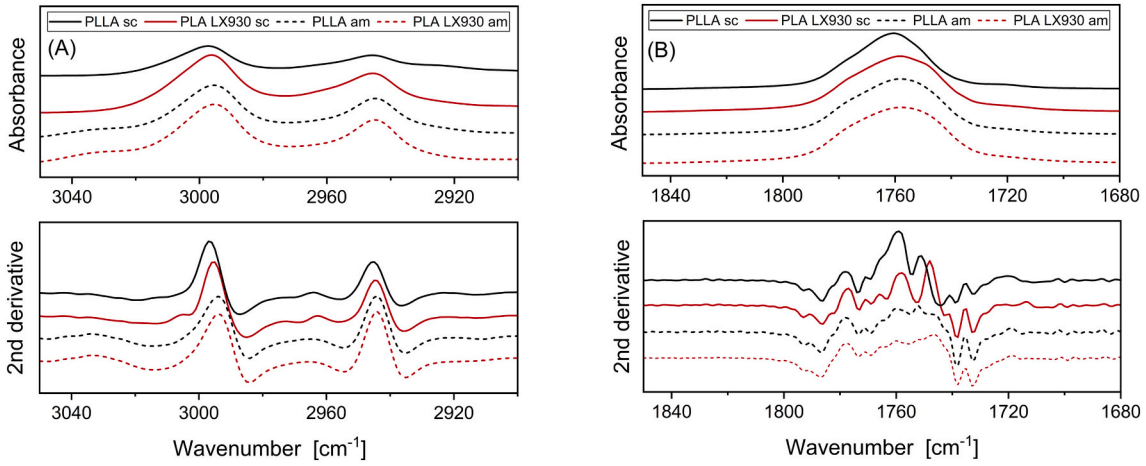

Fig. 7. FT-IR spectra of semi-crystalline PLLA (PLLA sc), semi-crystalline PLA LX930 (PLA LX930 sc), amorphous PLLA (PLLA am) and amorphous PLA LX930 (PLA LX930 am) in the (A) 3050–2900 cm^{-1} and (B) 1850–1680 cm^{-1} wavenumber regions.

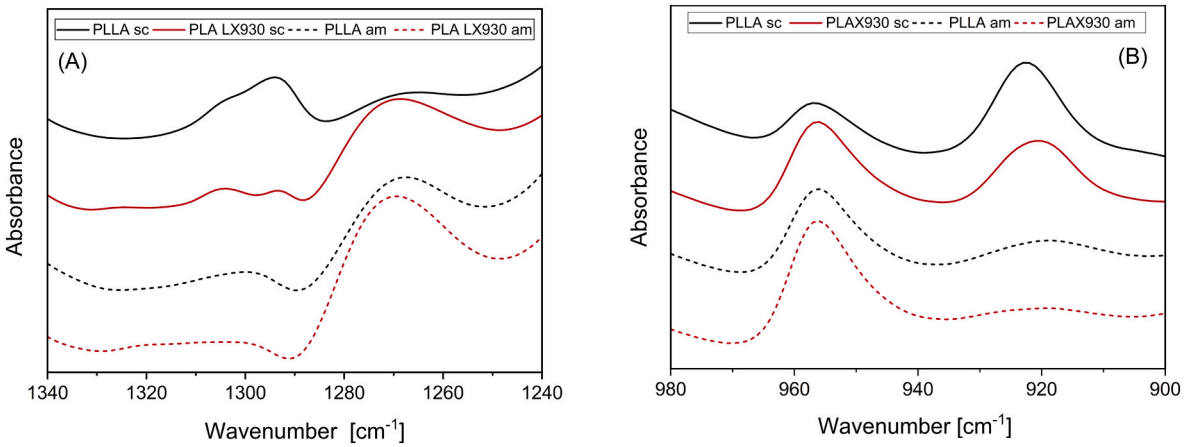

Fig. 8. FTIR spectra of semi-crystalline PLLA (PLLA sc), semi-crystalline PLA LX930 (PLA LX930 sc), amorphous PLLA (PLLA am) and amorphous PLA LX930 (PLA LX930 am) in the (A) 1340–1240 cm^{-1} and (B) 980–900 cm^{-1} wavenumber regions.

Fig. 7(A) and (B) compares the FT-IR spectra of semi-crystalline PLLA and PLA LX 930 together with the relative second derivatives in the wavenumber regions of 3050–2900 cm^{-1} and 1850–1680 cm^{-1}. In the Figure also the spectra of the amorphous samples are plotted for reference. The FT-IR curve of semi-crystalline PLA LX930 in the frequency range 3050–2900 cm^{-1} (Fig. 7(A)) displays that the main peak is located at slightly lower frequency with respect to semi-crystalline PLLA (see second derivatives). This peak, which corresponds to the asymmetric CH_3 stretching, is located at 2996 cm^{-1} in semi-crystalline PLLA containing α-crystals [55] and at slightly lower frequency (about 1 cm^{-1}) in the PLLA/PDLA stereocomplex [55,56]. The region of the C=O stretching (Fig. 7(B)) also shows (see second derivatives) a shift of some components of the overall peak towards lower wavenumbers. It has been reported that for semi-crystalline PLLA with α-crystals the peak linked to the carbonyl stretching consists of four components at 1749 (here 1751), 1759, which is the most intense, 1767 and 1776 cm^{-1}, which were assigned to tt, gt, tg and gg conformers, respectively [55,57]. In PLLA/PDLA stereocomplex, the most intense component is located at lower frequency, i.e. 1749 cm^{-1} [55], the same frequency at which the most intense component is observed in semi-crystalline PLA LX930. From the comparison of the intensities of the second derivatives it can be deduced that tt conformer prevails in the semi-crystalline PLA LX930, whereas

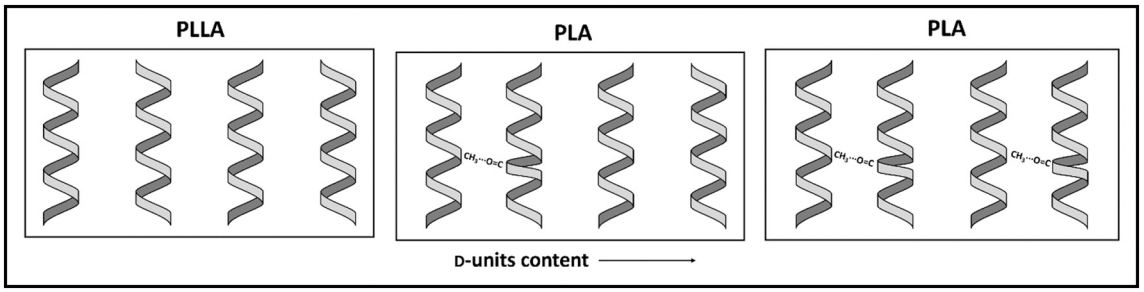

Fig. 9. Schematic representation of the possible effect of the D-units incorporation on the PLA helical crystal structure.

the gt conformer predominates in semi-crystalline PLLA. For semi-crystalline PLA LX930, the occurring of red shift for the CH_3 stretching band and the change in the most intense component of the C=O stretching confirms that CH_3···O=C interactions, which are massively present in the PLLA/PDLA stereocomplex [56], are active also in the PLA copolymers.

The analysis of the FT-IR curves in the 1340–1240 cm^{-1} and 980–900 cm^{-1} regions (Fig. 8(A) and (B)) further proves that the crystal structure of PLA LX930 tends slightly to that of the PLLA/PDLA stereocomplex. The 1340–1240 cm^{-1} region is assigned to symmetric CH_3 bending + C-H bending + C–O–C stretching modes [58,59]. Semi-crystalline PLLA displays two peaks, at 1304 and 1293 cm^{-1}. The intensity of the peak at 1293 cm^{-1} appears strongly reduced in the semi-crystalline PLA LX930. By taking into account that this band is completely absent in the PLLA/PDLA stereocomplex, it can be assessed that a certain resemblance exists between the crystal phase of PLA LX930 and the stereocomplex.

Differences in the FT-IR bands can be detected also in the 980–900 cm^{-1} region, specific of C-C backbone stretching + CH_3 rocking modes [55,59]. The peak at 921 cm^{-1}, which is typical of the 10_3 helix conformation of semi-crystalline PLLA, shifts to slightly lower frequency in the semi-crystalline PLA LX930, in agreement with the shift to 908 cm^{-1} observed for the PLLA/PDLA stereocomplex [55,59].

In conclusion, all the present experimental findings prove that the D-units are not completely excluded from the crystals of the PLA copolymers, thus confirming the results presented many years ago by Fischer et al. [21] and contradicted more recently in other studies [18–20]. The phenomenon, which pertains to copolymers and is called isodimorphism, represents an intermediate situation between total comonomer inclusion and total comonomer exclusion [22,23].

The progressive decrease in the melting temperature with increasing the D-units percentage attests that the D-units are included in the PLLA crystal lattice as defects (see Table 3). It has been here proven that the insertion of D-units in the crystal cell introduces additional interactions between the crystalline PLA segments. On the other hand, this incorporation certainly also modifies locally the helical chains conformations typical of the PLLA α-phase, with the result that defective crystalline structures with reduced melting temperatures are produced. A schematic representation of the possible effect of the D-units incorporation on the PLA crystal structure is sketched in Fig. 9. Contraction in the lattice dimensions and T_m decrease are not in contradiction. Examples of copolymers in which the partial inclusion of co-units produces a shrinkage in the crystal lattice and a simultaneous decrease in T_m have been reported and interpreted as cases of isodimorphism [22,23,60–62].

4. Conclusions

The focus of this study was the investigation of the crystal structure of PLA copolymers as a function of the D-units content. Additionally, the impact of the D-units on the amorphous interphase located at the amorphous/crystal boundary was analysed.

Semi-crystalline PLLA and PLA copolymers with different crystallinity were prepared and the various fractions (i.e.: w_{MAF}, w_C and w_{RAF}) quantified. The crystallinity decrease, observed with increasing the D-units content, was found to be correlated with a rise in MAF and a decrease in RAF.

The general trend of the RAF evolution was confirmed: RAF generally increases during the crystallization process, reaching a maximum and then slightly decreases in parallel to the final progressive perfection of the crystals. Moreover, the w_{RAF}/w_C ratio quantification highlighted quite similar values for PLLA and PLA copolymers, indicating that the D-units do not substantially affect the RAF thickness. The finding suggested that the D-units are not completely excluded from the crystals.

Inclusion of D-units in the crystal lattice as defects was indeed confirmed by XRD spectra. The analysis disclosed that the D-units inclusion occurs progressively and that the crystal phase gets gradually richer in D-units as the crystallization time evolves. The incorporation of D-units in the crystal phase can be promoted by the formation of local CH_3···O=C interactions, similar to those massively active between the PLLA and the PDLA chains in the PLA stereocomplex. The establishment of these interactions leads to a contraction of the interplanar distances and a progressive decrease in the crystal cell volume as the crystallization time and the D-units percentage increase. The presence of local CH_3···O=C interactions in the PLA copolymers was also confirmed by FT-IR investigation.

CRediT authorship contribution statement

Giovanna Molinari: Writing – review & editing, Writing – original draft, Validation, Investigation, Formal analysis, Data curation. **Paola Parlanti:** Writing – review & editing, Investigation. **Elisa Passaglia:** Writing – review & editing, Validation, Investigation, Formal analysis, Data curation. **Federica Aiello:** Data curation, Formal analysis, Investigation, Writing – review & editing. **Mauro Gemmi:** Writing – review & editing, Validation, Funding acquisition. **Andrea Lazzeri:** Writing – review & editing, Validation, Funding acquisition. **Maria Cristina Righetti:** Writing – review & editing, Writing – original draft, Validation, Supervision, Methodology, Investigation, Formal analysis, Data curation, Conceptualization.

Declaration of competing interest

The authors declare that they have no known competing financial interests or personal relationships that could have appeared to influence the work reported in this paper.

Data availability

The data that support the findings of the present study are available from the corresponding author upon reasonable request.

Acknowledgement

CISUP (Center for Instrument Sharing-University of Pisa) is acknowledged for the use of the Bruker Avance Neo 700 NMR spectrometer. E.P. is grateful to MICS (Made in Italy – Circular and Sustainable) Extended Partnership funded by the European Union Next-GenerationEU (PIANO NAZIONALE DI RIPRESA E RESILIENZA (PNRR) – MISSIONE 4 COMPONENTE 2, INVESTIMENTO 1.3 – D. D.1551.11-10-2022, PE00000004). This manuscript reflects only the authors' views and opinions, neither the European Union nor the European Commission can be considered responsible for them.

Appendix A. Supplementary data

Supplementary data to this article can be found online at https://doi.org/10.1016/j.ijbiomac.2024.136296.

References

[1] European Bioplastics, Bioplastic materials. https://www.european-bioplastics.org/bioplastics/materials/.
[2] R. Auras, B. Harte, S. Selke, An overview of polylactides as packaging materials, Macromol. Biosci. 4 (2004) 835–864, https://doi.org/10.1002/mabi.200400043.
[3] L.T. Lim, R. Auras, M. Rubino, Processing technologies for poly(lactic acid), Prog. Polym. Sci. 33 (2008) 820–852, https://doi.org/10.1016/j.progpolymsci.2008.05.004.
[4] A.P. Gupta, V. Kumar, New emerging trends in synthetic biodegradable polymers - Polylactide: a critique, Eur. Polym. J. 43 (2007) 4053–4074, https://doi.org/10.1016/j.eurpolymj.2007.06.045.
[5] D. Garlotta, A literature review of poly(lactic acid), J. Polym. Environ. 9 (2001) 63–84, https://doi.org/10.1023/A:1020200822435.
[6] S. Saeidlou, M.A. Huneault, H. Li, C.B. Park, Poly(lactic acid) crystallization, Prog. Polym. Sci. 37 (2012) 1657–1677, https://doi.org/10.1016/j.progpolymsci.2012.07.005.

[7] H.T. Rafael Auras, Loong-Tak Lim, Susan E.M. Selke, Poly(lactic acid): synthesis, structures, properties, Processing, and Applications, Wiley (2010), https://doi.org/10.1002/9780470649848.

[8] B. Lotz, Crystal polymorphism and morphology of polylactides, Adv. Polym. Sci. 279 (2018) 273–302, https://doi.org/10.1007/12_2016_15.

[9] P. Pan, Y. Inoue, Polymorphism and isomorphism in biodegradable polyesters, Prog. Polym. Sci. 34 (2009) 605–640, https://doi.org/10.1016/j.progpolymsci.2009.01.003.

[10] R. Androsch, C. Schick, M.L. Di Lorenzo, Melting of Conformationally disordered crystals (α'-phase) of poly(L-lactic acid), Macromol. Chem. Phys. 215 (2014) 1134–1139, https://doi.org/10.1002/macp.201400126.

[11] R. Androsch, E. Zhuravlev, C. Schick, Solid-state reorganization, melting and melt-recrystallization of conformationally disordered crystals (α'-phase) of poly (L-lactic acid), Polymer 55 (2014) 4932–4941, https://doi.org/10.1016/j.polymer.2014.07.046.

[12] J. Zhang, K. Tashiro, H. Tsuji, A.J. Domb, Disorder-to-order phase transition and multiple melting behavior of poly(L-lactide) investigated by simultaneous measurements of WAXD and DSC, Macromolecules 41 (2008) 1352–1357, https://doi.org/10.1021/ma0706071.

[13] R. Androsch, M.L. Di Lorenzo, C. Schick, Crystal nucleation in random L/D-lactide copolymers, Eur. Polym. J. 75 (2016) 474–485, https://doi.org/10.1016/j.eurpolymj.2016.01.020.

[14] M.L. Di Lorenzo, P. Rubino, R. Luijkx, M. Hélou, Influence of chain structure on crystal polymorphism of poly(lactic acid). Part 1: effect of optical purity of the monomer, Colloid Polym. Sci. 292 (2014) 399–409, https://doi.org/10.1007/s00396-013-3081-z.

[15] P. Song, L. Sang, C. Jin, Z. Wei, Temperature-dependent polymorphic crystallization of poly(L-lactide)s on the basis of optical purity and microstructure, Polymer 134 (2018) 163–174, https://doi.org/10.1016/j.polymer.2017.11.069.

[16] E. Blázquez-Blázquez, R. Barranco-García, T.M. Díez-Rodríguez, M.L. Cerrada, E. Pérez, Combined effects from dual incorporation of ATBC as plasticizer and mesoporous MCM-41 as nucleating agent on the PLA isothermal crystallization in environmentally-friendly ternary composite systems, Polymers (Basel) 15 (2023) 624, https://doi.org/10.3390/polym15030624.

[17] H. Abe, M. Harigaya, Y. Kikkawa, T. Tsuge, Y. Doi, Crystal growth and solid-state structure of poly(lactide) Stereocopolymers, Biomacromolecules 6 (2005) 457–467, https://doi.org/10.1021/bm049497l.

[18] J. Cho, S. Baratian, J. Kim, F. Yeh, B.S. Hsiao, J. Runt, Crystallization and structure formation of poly(L-lactide-*co*-*meso*-lactide) random copolymers: a time-resolved wide- and small-angle X-ray scattering study, Polymer 44 (2003) 711–717, https://doi.org/10.1016/S0032-3861(02)00823-6.

[19] J. Huang, M.S. Lisowski, J. Runt, E.S. Hall, R.T. Kean, N. Buehler, J.S. Lin, Crystallization and microstructure of poly(L-lactide-*co*-*meso*-lactide) copolymers, Macromolecules 31 (1998) 2593–2599, https://doi.org/10.1021/ma9714629.

[20] S. Baratian, E.S. Hall, J.S. Lin, R. Xu, J. Runt, Crystallization and solid-state structure of random polylactide copolymers: poly(L-lactide-*co*-D-lactide)s, Macromolecules 34 (2001) 4857–4864, https://doi.org/10.1021/ma001125r.

[21] E.W. Fischer, H.J. Sterzel, G. Wegner, Investigation of the structure of solution grown crystals of lactide copolymers by means of chemical reactions, Kolloid-Zeitschrift Und Zeitschrift Für Polym. 251 (1973) 980–990, https://doi.org/10.1007/BF01498927.

[22] R.A. Pérez-Camargo, I. Arandia, M. Safari, D. Cavallo, N. Lotti, M. Soccio, A. J. Müller, Crystallization of isodimorphic aliphatic random copolyesters: Pseudo-eutectic behavior and double-crystalline materials, Eur. Polym. J. 101 (2018) 233–247, https://doi.org/10.1016/j.eurpolymj.2018.02.037.

[23] R.A. Pérez-Camargo, M. Safari, J. Torres Rodríguez, Y. Liao, A.J. Müller, Structure, morphology and crystallization of isodimorphic random copolymers: copolyesters, copolycarbonates and copolyamides, Polymer 287 (2023) 126412, https://doi.org/10.1016/j.polymer.2023.126412.

[24] B. Wunderlich, Reversible crystallization and the rigid amorphous phase in semicrystalline macromolecules, Prog. Polym. Sci. 28 (2003) 383–450, https://doi.org/10.1016/S0079-6700(02)00085-0.

[25] M.C. Righetti, D. Prevosto, E. Tombari, Time and temperature evolution of the rigid amorphous fraction and differently constrained amorphous fractions in PLLA, Macromol. Chem. Phys. 217 (2016) 2013–2026, https://doi.org/10.1002/macp.201600210.

[26] M.C. Righetti, Amorphous fractions of poly(lactic acid), Adv. Polym. Sci. 279 (2018) 195–234, https://doi.org/10.1007/12_2016_14.

[27] D.S. Simmons, An emerging unified view of dynamic interphases in polymers, Macromol. Chem. Phys. 217 (2016) 137–148, https://doi.org/10.1002/macp.201500284.

[28] R. Rastogi, W.P. Vellinca, S. Rastogi, C. Schick, H.E.H. Meijer, The three-phase structure and mechanical properties of poly(ethylene terephthalate), J. Polym. Sci. Part B Polym. Phys. 42 (2004) 2092–2106, https://doi.org/10.1002/polb.20096.

[29] P.J. In 't Veld, M. Hütter, G.C. Rutledge, Temperature-dependent thermal and elastic properties of the interlamellar phase of semicrystalline polyethylene by molecular simulation, Macromolecules 39 (2006) 439–447, https://doi.org/10.1021/ma0518961.

[30] A. Sedighiamiri, T.B. Van Erp, G.W.M. Peters, L.E. Govaert, J.A.W. van Dommelen, Micromechanical modeling of the elastic properties of semicrystalline polymers: a three-phase approach, J. Polym. Sci. Part B Polym. Phys. 48 (2010) 2173–2184, https://doi.org/10.1002/polb.22099.

[31] Product Data Sheet Luminy® L175. https://www.totalenergies-corbion.com/media/eushodia/pds-luminy-l175-190507.pdf, 2017.

[32] https://www.natureworksllc.com/~/media/Files/NatureWorks/Technical-Documents/Properties-Documents/PropertiesDocument_Solubility-Test-Results_pdf.pdf?la=en.

[33] Product Data Sheet Luminy® LX930. https://www.totalenergies-corbion.com/media/otwa3abw/pds-luminy-lx930-211013.pdf.

[34] S.M. Sarge, W. Hemminger, E. Gmelin, G.W.H. Höhne, H.K. Cammenga, W. Eysel, Metrologically based procedures for the temperature, heat and heat flow rate calibration of DSC, J. Thermal Anal. 49 (1997) 1125–1134, https://doi.org/10.1007/BF01996802.

[35] A. Wurm, M. Merzlyakov, C. Schick, Reversible melting probed by temperature modulated dynamic mechanical and calorimetric measurements, Colloid Polym. Sci. 276 (1998) 289–296, https://doi.org/10.1007/s003960050242.

[36] R. Androsch, I. Moon, S. Kreitmeier, B. Wunderlich, Determination of heat capacity with a sawtooth-type, power-compensated temperature-modulated DSC, Thermochim. Acta 357–358 (2000) 267–278, https://doi.org/10.1016/S0040-6031(00)00397-X.

[37] M. Pyda, B. Wunderlich, Reversing and nonreversing heat capacity of poly(lactic acid) in the glass transition region by TMDSC, Macromolecules 38 (2005) 10472–10479, https://doi.org/10.1021/ma051611k.

[38] M.L. Di Lorenzo, B. Wunderlich, Temperature-modulated calorimetry of the crystallization of polymers analyzed by measurements and model calculations, J. Therm. Anal. Calorim. 57 (1999) 459–472, https://doi.org/10.1023/A:1010163923965.

[39] P. Pan, B. Zhu, W. Kai, T. Dong, Y. Inoue, Polymorphic transition in disordered poly (L-lactide) crystals induced by annealing at elevated temperatures, Macromolecules 41 (2008) 4296–4304, https://doi.org/10.1021/ma800343g.

[40] T. Kawai, N. Rahman, G. Matsuba, K. Nishida, T. Kanaya, M. Nakano, H. Okamoto, J. Kawada, A. Usuki, N. Honma, K. Nakajima, M. Matsuda, Crystallization and melting behavior of poly (L-lactic acid), Macromolecules 40 (2007) 9463–9469, https://doi.org/10.1021/ma070082c.

[41] M.C. Righetti, M. Gazzano, M.L. Di Lorenzo, R. Androsch, Enthalpy of melting of α'- and α-crystals of poly(L-lactic acid), Eur. Polym. J. 70 (2015) 215–220, https://doi.org/10.1016/j.eurpolymj.2015.07.024.

[42] K. Jariyavidyanont, M. Du, Q. Yu, T. Thurn-Albrecht, C. Schick, R. Androsch, Bulk enthalpy of melting of poly (L-lactic acid) (PLLA) determined by fast scanning Chip calorimetry, Macromol. Rapid Commun. 43 (2022) 1–10, https://doi.org/10.1002/marc.202200148.

[43] R. Androsch, B. Wunderlich, The link between rigid amorphous fraction and crystal perfection in cold-crystallized poly(ethylene terephthalate), Polymer 46 (2005) 12556–12566, https://doi.org/10.1016/j.polymer.2005.10.099.

[44] M.L. Di Lorenzo, M.C. Righetti, Effect of thermal history on the evolution of crystal and amorphous fractions of poly[(R)-3-hydroxybutyrate] upon storage at ambient temperature, Eur. Polym. J. 49 (2013) 510–517, https://doi.org/10.1016/j.eurpolymj.2012.11.004.

[45] M.L. Di Lorenzo, R. Androsch, M.C. Righetti, The irreversible form II to form I transformation in random butene-1/ethylene copolymers, Eur. Polym. J. 67 (2015) 264–273, https://doi.org/10.1016/j.eurpolymj.2015.04.002.

[46] M.F.C. Ladd, In Structure Determination by X-ray Crystallography, 2nd ed., 1985, p. 65.

[47] Z.-G. Wang, X. Wang, B.S. Hsiao, S. Andjelić, D. Jamiolkowski, J. McDivitt, J. Fischer, J. Zhou, C.C. Han, Time-resolved isothermal crystallization of absorbable PGA-*co*-PLA copolymer by synchrotron small-angle X-ray scattering and wide-angle X-ray diffraction, Polymer 42 (2001) 8965–8973, https://doi.org/10.1016/S0032-3861(01)00374-3.

[48] K. Tashiro, H. Wang, N. Kouno, J. Koshobu, K. Watanabe, Confirmation of the X-ray-analyzed heterogeneous distribution of the PDLA and PLLA chain stems in the crystal lattice of poly(lactic acid) Stereocomplex on the basis of the vibrational circular dichroism IR spectral measurement, Macromolecules 50 (2017) 8066–8071, https://doi.org/10.1021/acs.macromol.7b01573.

[49] K. Wasanasuk, K. Tashiro, M. Hanesaka, T. Ohhara, K. Kurihara, R. Kuroki, T. Tamada, T. Ozeki, T. Kanamoto, Crystal structure analysis of poly(L-lactic acid) α form on the basis of the 2-dimensional wide-angle synchrotron X-ray and neutron diffraction measurements, Macromolecules 44 (2011) 6441–6452, https://doi.org/10.1021/ma2006624.

[50] H. Tsuji, Poly(lactide) stereocomplexes: formation, structure, properties, degradation, and applications, Macromol. Biosci. 5 (2005) 569–597, https://doi.org/10.1002/mabi.200500062.

[51] D. Sawai, Y. Tsugane, M. Tamada, T. Kanamoto, M. Sungil, S. Hyon, Crystal density and heat of fusion for a stereo-complex of poly(L-lactic acid) and poly(D-lactic acid), J. Polym. Sci. Part B Polym. Phys. 45 (2007) 2632–2639, https://doi.org/10.1002/polb.21270.

[52] J. Zhang, H. Sato, H. Tsuji, I. Noda, Y. Ozaki, Differences in the $CH_3\cdots O{=}C$ interactions among poly(L-lactide), poly(L-lactide)/poly(D-lactide) stereocomplex, and poly(3-hydroxybutyrate) studied by infrared spectroscopy, J. Mol. Struct. 735–736 (2005) 249–257, https://doi.org/10.1016/j.molstruc.2004.11.033.

[53] W. Chen, D. Reichert, T. Miyoshi, Helical jump motions of poly(L-lactic acid) chains in the α phase as revealed by solid-state NMR, J. Phys. Chem. B 119 (2015) 4552–4563, https://doi.org/10.1021/acs.jpcb.5b00694.

[54] W. Chen, W. Zhou, Y. Makita, S. Wang, S. Yuan, T. Konishi, T. Miyoshi, Characterization of the slow molecular dynamics of poly(L-lactic acid) in α and α' phases, in a glassy state, and in a complex with poly(D-lactic acid) by solid-state NMR, Macromol. Chem. Phys. 219 (2018) 1700451, https://doi.org/10.1002/macp.201700451.

[55] P. Pan, J. Yang, G. Shan, Y. Bao, Z. Weng, A. Cao, K. Yazawa, Y. Inoue, Temperature-variable FTIR and solid-state ^{13}C NMR investigations on crystalline structure and molecular dynamics of polymorphic poly(L-lactide) and poly(L-

lactide)/poly(D-lactide) stereocomplex, Macromolecules 45 (2012) 189–197, https://doi.org/10.1021/ma201906a.
[56] J. Zhang, H. Sato, H. Tsuji, I. Noda, Y. Ozaki, Infrared spectroscopic study of CH_3 ···O=C interaction during poly(L-lactide)/poly(D-lactide) Stereocomplex formation, Macromolecules 38 (2005) 1822–1828, https://doi.org/10.1021/ma047872w.
[57] E. Meaurio, N. López-Rodríguez, J.R. Sarasua, Infrared spectrum of poly(L-lactide): application to crystallinity studies, Macromolecules 39 (2006) 9291–9301, https://doi.org/10.1021/ma061890r.
[58] N.M. Praveena, G. Virat, V.G. Krishnan, E.B. Gowd, Stereocomplex formation and hierarchical structural changes during heating of supramolecular gels obtained by polylactide racemic blends, Polymer 241 (2022) 124530, https://doi.org/10.1016/j.polymer.2022.124530.
[59] N.M. Praveena, P. Shaiju, R.B.A. Raj, E.B. Gowd, Infrared bands to distinguish amorphous, meso and crystalline phases of poly(lactide)s: crystallization and phase transition pathways of amorphous, meso and co-crystal phases of poly(L-lactide) in the heating process, Polymer 240 (2022) 124495, https://doi.org/10.1016/j.polymer.2021.124495.
[60] Y. Yu, Z. Wei, L. Zheng, C. Jin, X. Leng, Y. Li, Competition and miscibility of isodimorphism and their effects on band spherulites and mechanical properties of poly(butylene succinate-co-cis-butene succinate) unsaturated aliphatic copolyesters, Polymer 150 (2018) 52–63, https://doi.org/10.1016/j.polymer.2018.07.024.
[61] R.A. Pérez-Camargo, G. Liu, D. Cavallo, D. Wang, A.J. Müller, Effect of the crystallization conditions on the exclusion/inclusion balance in biodegradable poly (butylene succinate- *ran* -butylene adipate) copolymers, Biomacromolecules 21 (2020) 3420–3435, https://doi.org/10.1021/acs.biomac.0c00847.
[62] Y. Yu, L. Sang, Z. Wei, X. Leng, Y. Li, Unique isodimorphism and isomorphism behaviors of even-odd poly(hexamethylene dicarboxylate) aliphatic copolyesters, Polymer 115 (2017) 106–117, https://doi.org/10.1016/j.polymer.2017.03.034.